Oxidation of Metals, Vol. 65, Nos. 1/2, February 2006 (© 2006)
DOI: 10.1007/s11085-006-9002-5

Pre-oxidation of Inconel Alloys for Inhibition of Carbon Deposition from Heated Jet Fuel

Orhan Altin* and Semih Eser*†

Received June 9, 2005; revised August 29, 2005

Exposure of superalloy surfaces to jet fuel at elevated temperatures leads to the formation of carbonaceous deposits and metal sulfides. The formation of stable oxide layers on alloy surfaces can reduce the activity of the constituent transition metals that catalyze the dehydrogenation of hydrocarbons and the subsequent carbon deposit growth. The metals Ni, Cr, Fe, Mn, Al, Ti and Nb + Ta form thermodynamically stable oxide layers after oxidation above 800°C under O_2 flow. In this study, we investigated the formation of oxides and spinels on three different Ni-base superalloys (Inconel 600, Inconel 718, and Inconel X750) and their activity towards carbon and sulfur deposit formation from jet fuel (JP-8) thermal stressing at 600°C and 34 atm (500 psig) for 5 hr. Metal oxide formation during pre-oxidation and the behavior of pre-oxidized samples in thermal stressing were found to depend strongly on the minor element composition of these superalloys.

KEY WORDS: Inconel alloys; carbon deposition; oxidation; sulfidation; jet fuel; thermal stability.

INTRODUCTION

Jet fuel is presently used as a coolant in military aircraft, in addition to its primary use as a propellant. It is used to cool the lubrication system, avionics, electrical systems, and environmental control systems, and is also used as a hydraulic fluid.[1] The trend of advanced aircraft toward

*Department of Energy and Geo-Environmental Engineering and the Energy Institute, Pennsylvania State University, 101 Hosler Building, University Park, PA 16802, USA.
†To whom correspondence should be sent. Tel.: +814-863-1392; Fax: +814-865-3248; e-mail: sxe2@psu.edu

increasing performance results in higher thermal loads and higher fuel temperatures that eventually lead to the formation of carbon deposits in fuel lines. The buildup of deposits in aircraft fuel systems is a major concern because it may lead to fuel system failure. Exposure of metal surfaces to jet fuel at temperatures higher than 400°C lead to carbonaceous deposits.[2,3] Various metal alloys were examined to study their activity in carbon deposit formation from jet fuel decomposition. The alloys studied consists mainly of commercial superalloys, such as Inconel 600, Inconel 718, Inconel X750, Fecralloy, Havar, Waspaloy, Hastelloy-C, and Mo–Re alloy. Among these alloys, Inconel X750 and Inconel 718 collected the least amount of deposit at 500 and 600°C during jet fuel stressing experiments.[4]

The examination of solid deposits collected on the surfaces of different alloys indicated that the hydrocarbon environment and the surface elemental composition of the alloys play a dominant role in controlling the extent of deposit formation. Filamentous deposit (most deleterious) is formed by the diffusion of carbon through the bulk of the alloy after catalytic dehydrogenation of hydrocarbons on the surface. Filamentous carbon grows from the surface with or without a metal tip.[5,6] In other cases, polyaromatic hydrocarbons produced in the fluid phase adsorb on the metal surface and lead to pyrolytic carbon growth, or mesophase formation.[7] The catalytic role of alloy surfaces in promoting carbon deposition can be suppressed by coating the surface with silica,[8] Silcosteel,[9] or by using other alternatives such as chromium plating,[10] TiO_2,[11] or MCrAlY coating.[12] Silica coating has been proved to be effective in reducing the deposit formation from jet fuel[13] and ethylene steam cracking.[14] It has been reported that the oxidation of chromium, aluminum, and titanium containing alloys can produce protective oxide layers that inhibit the carbon deposit formation.[15]

Inconel 600, Inconel X and Inconel 718 are all Ni based superalloys that are used for high temperature and corrosive environment industrial applications. The oxidation behavior of superalloys has been studied in detail by several authors.[16–22] It appears that the presence of Nb, Ta, Ti, and Al as minor components in superalloys affects their surface reactivity[13] and mechanical properties.[23] The addition of Al and Ti, for example, improves the mechanical properties of Ni-based alloys through the formation of γ' [Ni_3 (Al, Ti)] as the principal hardening precipitates.[23] Elliot and Hampton[24] reported, on the other hand, a considerable improvement in the oxidation resistance of a Ni–10%Cr alloy at 1000°C upon adding Nb and Ta to the binary alloy.

McIntyre *et al.*[17] studied the oxidation of Inconel 600 alloy in the temperature range of 100–700°C and discussed the formation of

$NiO–Cr_2O_3$, $NiFe_2O_4$ and CrO_2 at different temperatures and oxygen concentrations. Lenglet *et al.*[18] studied the initial stages (1–60 min) of oxidation of Inconel 718 in air between 100 and 1000°C and found that mostly Cr_2O_3, $NiCr_2O_4$ spinel and $NiFe_{2-x}Cr_xO_4$ $(0 < x < 1)$ formed in the oxide layer. Kumar *et al.*[19] have studied the oxidation behavior of Inconel 625 between 600 and 1250°C during the early stages (<150 min) at oxygen pressures of 0.12 and 101.3 kPa. The authors observed the enrichment of Cr_2O_3 oxide film above 600°C, the degree of enrichment was maximum at about 950°C and at temperatures above 1000°C, significant amounts of Nb and Ti oxides formed. Durasso and Ramanathan[20] studied the kinetics and formation of multilayered oxides on some Inconel alloys between 600 and 1000°C and identified an outer layer of NiO, intermediate layer of Ni-rich Ni–Cr oxide and an inner layer of Cr_2O_3.

In addition to hydrocarbon decomposition, the presence of organosulfur compounds plays a significant role in solid deposition on metal alloy surfaces. Sulfur compounds are universal contaminants in hydrocarbon fuels. Typically, a commercial jet fuel may contain between 300 and 2000 ppm of sulfur, distributed into thiols, thiophenes, disulfides, and polysulfides.[25] The effect of sulfur on carbon deposition seems to depend strongly on the chemical nature of the sulfur compounds. For example, Valenyi[26] found that the addition of H_2S in the steam-less ethane pyrolysis enhanced the coke deposition on an Inconel 600 tube. Reyners and Froment[27] also found that sulfur compounds promote coke formation in thermal cracking of hydrocarbons. These authors studied various sulfur compounds as additives and found that the carbon deposition rate decreases in the order dimethyl sulfide > carbon disulfide > benzothiophene > thiophene. In contrast, Tan and Baker,[28] reported that, over Fe–Ni particles, the carbon deposition from ethane/steam pyrolysis is inhibited by the presence of organic sulfides. On the other hand, Ohla and Grabke[29] reported that sulfur retard graphitic carbon formation on iron, but the growth of graphitic carbon on nickel was accelerated by sulfur. Trimm and Turner[30] observed both the facilitation and retardation effect of sulfur on carbon deposition from a mixture of propane and hydrogen on presulfided nickel, copper, iron and stainless steel surfaces. They suggested that the formation of stable metal sulfides on surfaces inhibited the carbon deposition, whereas the formation and subsequent decomposition of labile metal sulfides accelerated the deposition. The surface elemental composition of alloys controls the extent of metal sulfide formations. It has been noted that the addition of Cr and Al to iron decreases the sulfidaton rate, whereas Co and Ni addition had no effect on the sulfidation rate of iron.[31,32]

The objective of this study is to investigate the effects of oxidizing the Inconel 600, Inconel X750, and Inconel 718 surfaces on carbon deposit formation upon thermal stressing of jet fuel on these surfaces. These alloys were selected because of the differences in their major and minor element compositions and the differences observed in their behavior during thermal stressing with jet fuel.[4] The superalloys Inconel 600 and Inconel X750 have, for example, almost the same Ni content, but Inconel X750 alloy has minor additions of Al, Nb, Ta and Ti. Samples of superalloys were oxidized at 900°C under flowing O_2. The oxidized samples were examined by electron probe micro-analyzer (EPMA) and X-ray diffraction (XRD). Jet fuel thermal stressing on as-received and oxidized surfaces were conducted in a flow reactor and the solid deposits formed on different substrates were characterized by using a temperature-programmed oxidation (TPO) analysis, Field Emission Scanning Electron Microscopy (FESEM), and XRD.

EXPERIMENTAL PROCEDURES

Table I gives the nominal compositions of different alloys used in this study. While In 600 and In X750 alloys have similar base metal (Ni, Cr, Fe) content, they differ in minor element (e.g., Nb + Ta, Ti, and Al) concentrations. The In 718, on the other hand, has a much lower Ni, and higher Cr content than the other two alloys, but contains Mo, Al, Nb, Ta, and Ti as the principal minor elements. The foils of these alloys were cut to coupons with dimensions of 15 cm × 3 mm × 0.6 mm, and rinsed in acetone before the oxidation treatments. For oxidation, the foil samples were placed in a quartz boat and heated in an electric furnace to 900°C at a heating rate of 50°C/min and 101.3 kPa under flowing O_2 (150 mL/min) for 24 hr. The oxidized samples were allowed to cool down in the furnace under O_2 flow.

As-received and oxidized foils were thermally stressed with jet fuel in a flow reactor. The fuel used in this study was a JP-8 fuel which consists of 60% *n*-alkanes, 20% hydroaromatics and cycloalkanes, 18% aromatics, and 2% olefins. The distribution of the *n*-alkanes in the sample in the range from n-octane to *n*-heptadecane. The sulfur content of the JP-8

Table I. Bulk Composition of Superalloys (wt%) (Goodfellow, Inc.)

	Ni	Fe	Cr	Nb+Ta	Mo	Ti	Al	Cu	Mn	Si	C	S
In 600	74.4	8.0	15.5	—	—	—	—	0.5	1.0	0.5	0.15	0.0015
In 718	52.5	8.5	19.0	5.13	3.05	0.9	0.5	0.15	0.18	0.18	0.04	0.0008
In X	73.0	7.0	15.5	0.95	—	2.5	0.7	0.25	0.5	—	0.04	0.0005

fuel is 490 ppm, and the sulfur is distributed among several different types of organo-sulfur compounds, including dimethylbenzothiophenes and trimethyldibenzo-thiophenes as the principal sulfur species.

Thermal stressing of JP-8 was carried out at 600°C and 34 atm (500 psig) over the alloy foils for 5 hr at a liquid fuel flow rate of 4 mL/min. The alloy foil samples were placed in a 20 cm long and 1/4 in OD glass-lined stainless steel tube reactor. The isothermal tube reactor was heated conductively using an Inconel 600 heating block. A thermocouple placed in the middle of the reactor length and in contact with the external tube wall was used to control the reactor temperature. The inlet and outlet fluid temperatures were also measured by separate thermocouples. The fluid temperature at the outlet of the reactor was approximately 550°C, when the outside wall temperature was kept at 600°C. The details of the flow reactor set-up and the experimental procedure are described elsewhere.[33]

The carbon deposition on as-received and oxidized surfaces was measured quantitatively by using a LECO RC-412 multiphase carbon analyzer. The carbon deposits were oxidized under 750 mL/min O_2 flow by controlled heating from 100 to 900°C at a 30°C/min heating rate in a quartz furnace. Oxidation products CO_2 and CO and excess O_2 gas mixture flows through CuO catalyst bed for complete combustion of CO to CO_2. The amount of CO_2 evolution was quantitatively measured using calibrated IR detectors. Temperature Programmed Oxidation (TPO) profiles were plotted as the amount of CO_2 evolved versus the furnace temperature.

The alloy surfaces were examined by FESEM before and after the thermal stressing experiments. The oxidized foil cross sections were analyzed by EPMA to examine the oxide layers and the elemental maps. The surface oxide constituents of as-received, oxidized, and deposited surfaces were identified by XRD using Cu Kα ($\lambda = 1.5418$ Å) radiation. The X-ray patterns were examined using JCPDS files.

The carbon deposits were examined directly by FESEM/EDS and by a transmission electron microscope (TEM). For TEM, the stressed alloy foils were sonicated in ethanol, one drop of the dispersed solution was placed on a microgrid for observation.

RESULTS

The experimental results are presented in the two subsections that include the oxidation of the three superalloys and the thermal stressing of the as-received and oxidized surface with the jet fuel sample.

Oxidation of Alloy Surfaces

Under the same oxidation conditions, the three superalloy samples showed differences in the extent of oxidation and the composition of the oxide layers produced on the foil surfaces. Experimental results from the analyses of the as-received and oxidized foils are presented for each sample below.

Inconel 600

Figure 1 shows the XRD profiles of the as-received and oxidized surfaces of the Inconel 600 alloy. The XRD profiles of the as-received surface shows that Ni is dominantly present with small amounts of Cr and Fe oxides. After oxidation, however, the surface contains Cr_2O_3, Fe_2O_3, NiO, $NiCr_2O_4$, and $FeCr_2O_4$ oxides. The oxidation of Inconel 600 alloy resulted in a dark gray surface that displays a highly crystalline structure of nodules as shown in Fig. 2. The EPMA back-scattered and elemental images shown in Fig. 3 indicate that there are four different oxide layers formed on the Inconel 600 surface upon oxidation. The total oxide layer thickness was approximately $10\,\mu$. A combination of XRD and elemental EPMA maps showed that the top layer contains elemental Ni and Cr, NiO, Cr_2O_3, Fe_2O_3, and $NiCr_2O_4$ spinel, the second layer contains Cr_2O_3 rich in $FeCr_2O_4$ and $NiCr_2O_4$ spinels, and the third layer contains NiO with the presence of Fe and Cr oxides, and the fourth layer at the bottom consists of Cr_2O_3 only.

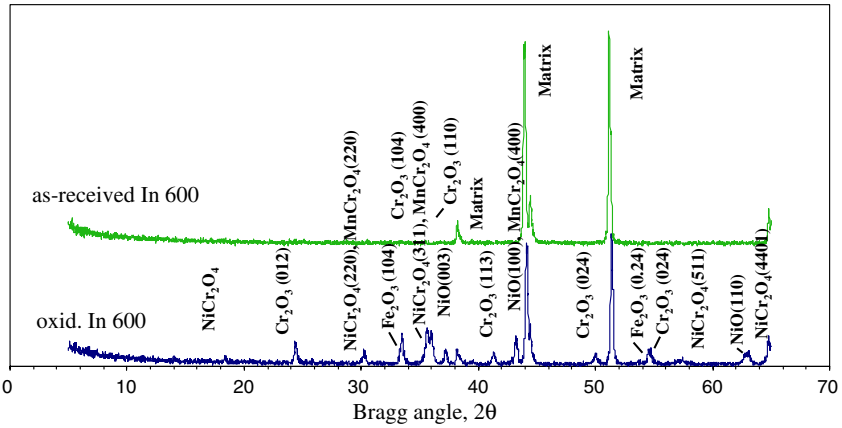

Fig. 1. X-ray diffraction patterns of as-received and oxidized Inconel 600 foils. Cu Kα ($\lambda = 1.5418$ Å) 40 kV–20 mA.

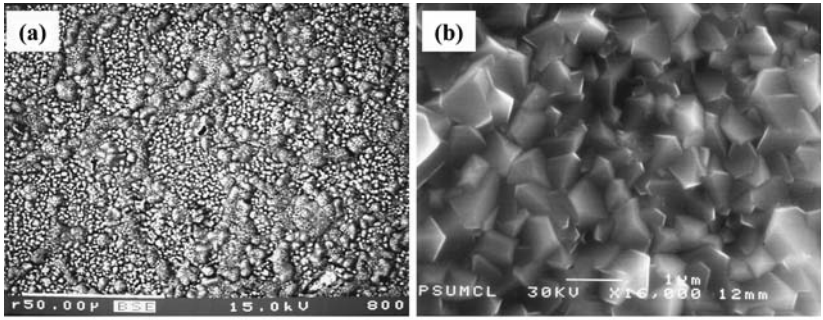

Fig. 2. EPMA back-scattered (×800) (a) and FESEM (×16, 000) (b) images of Inconel 600 surface after 24 hr oxidation at 900°C under 150 mL/min of O_2 flow.

Inconel 718

Figure 4 shows that as-received Inconel 718 surface contains mainly Ni, Cr in the elemental and oxides form, and Al_2O_3. After 24 hr oxidation at 900°C, the surface is enriched in Cr_2O_3, Al_2O_3 and TiO_2. Contrary to Inconel 600, Inconel 718 contains finer grains that range in size from 10 to 20 μ as shown in Fig. 5. Higher magnification images of the Inconel 718 surface indicates similar crystalline structures to those observed on the Inconel 600 surface. The Cr_2O_3, TiO_2 (rutile), and Al_2O_3 enrichments were identified by means of XRD and EPMA analysis. As seen in Fig. 6, three different oxide layers were formed by the diffusion of Cr, Al and Ti through the gas–solid interface. The total thickness of the oxide layers equals approximately 3 μ. The outer thinnest layer consists of Ni, NiO, Cr_2O_3, and $NiCr_2O_4$ spinel. The intermediate layer consists mostly of Cr_2O_3 with trace amounts of $FeCr_2O_4$, $NiCr_2O_4$, Fe_2O_3, Al_2O_3, TiO_2, and $Fe(Cr,Al)_2O_4$. The innermost layer is enriched with TiO_2, Al_2O_3 and the solid solution oxide (Ti, Nb, Ta, Fe)O_2. This third layer contains significantly higher amount of Ti as can be observed from the EPMA elemental maps. Figure 6 shows the presence of Al and O beneath the innermost scale, indicating an internal oxidation zone that contains the precipitates of Al_2O_3. The refractory metals, Ta and Nb, are also enriched in this layer.

Inconel X750

As different from the behavior of Inconel 600 and Inconel 718 alloys, Inconel X750 gave a more abundant formation of Cr_2O_3, TiO_2, and Al_2O_3 with a lower amount of $NiCr_2O_4$ spinel formation after oxidation (Fig. 7). Inconel X750 surface grain structure is similar to that of Inconel

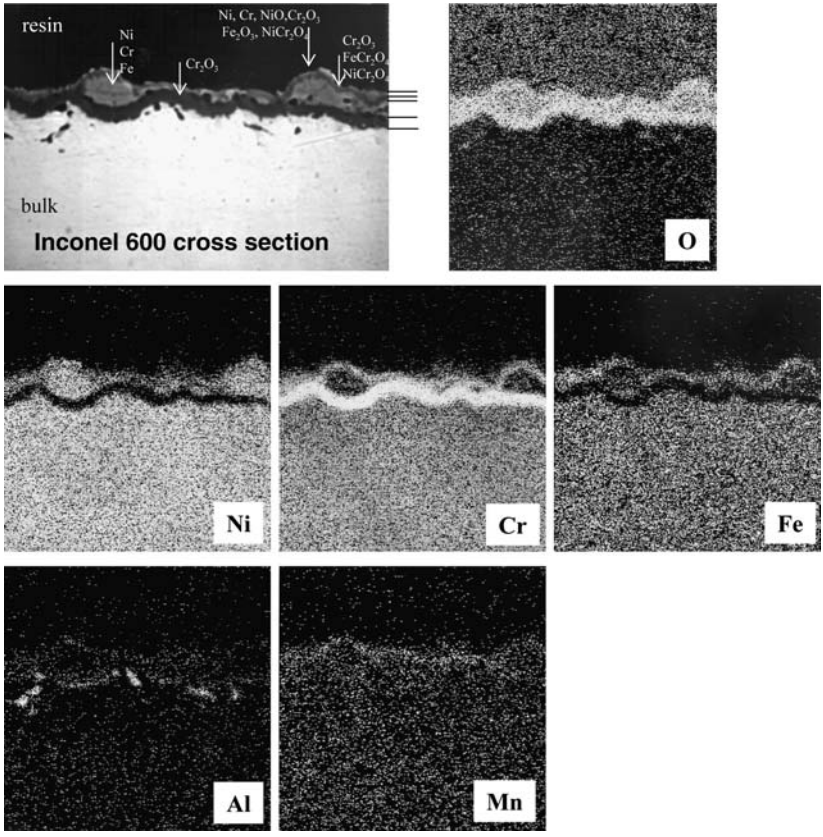

Fig. 3. EPMA back-scattered image for cross section of Inconel 600 showing oxide layers and elemental map images after 24 hr oxidation of alloy specimen at 900°C under 150 mL/min O_2 flow.

600 with the grains larger than 50 μ. The total thickness of the oxide layers is approximately 7 μ. Figure 8 shows that the external surface consists of porous nodules of oxides with almost complete absence of nickel in the top layer, as evident in the EPMA images of Fig. 9. Three layers of oxides were observed from the back-scattered images from the cross-section of the Inconel X foil. The outer layer consists mainly of Cr_2O_3 and TiO_2. The intermediate layer is rich in Cr_2O_3 with traces of Ni, Fe oxides, and $FeCr_2O_4$ and $NiCr_2O_4$ spinels. The third layer is composed of a continuous layer of Al_2O_3 and a solid solution of (Ti, Nb, Ta)O_2.

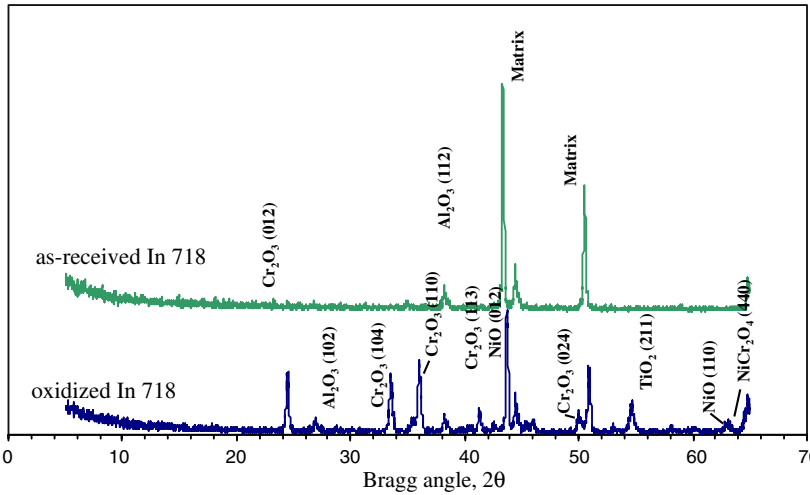

Fig. 4. X-ray diffraction patterns of as-received and oxidized Inconel 718 foils. Cu Kα ($\lambda = 1.5418$ Å) 40 kV–20 mA.

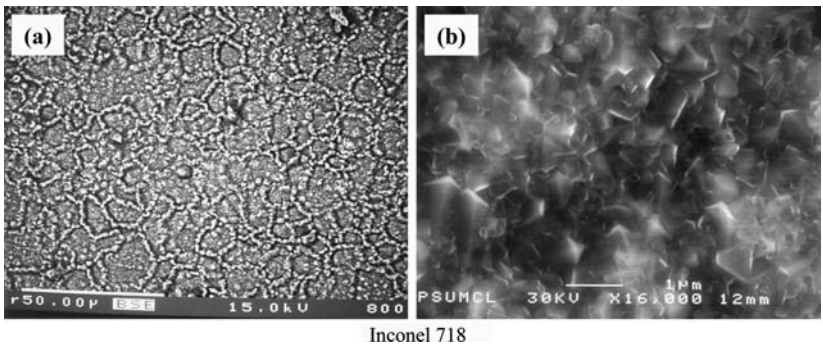

Fig. 5. EPMA back-scattered (×800) (a) and FESEM (×16, 000) (b) images of Inconel 718 surface after 24 hr oxidation at 900°C under 150 mL/min of O_2 flow.

Jet Fuel Stressing on As-received and Oxidized Surfaces

The oxidation treatment has significantly reduced the carbon deposition on the alloys, particularly on Inconel 600, upon stressing with JP-8. Table II compares the amount of carbon deposited on as-received and oxidized superalloy foils. The amount of deposits on Inconel 600 was reduced more than three-fold with more modest decreases on Inconel X750, and Inconel 718.

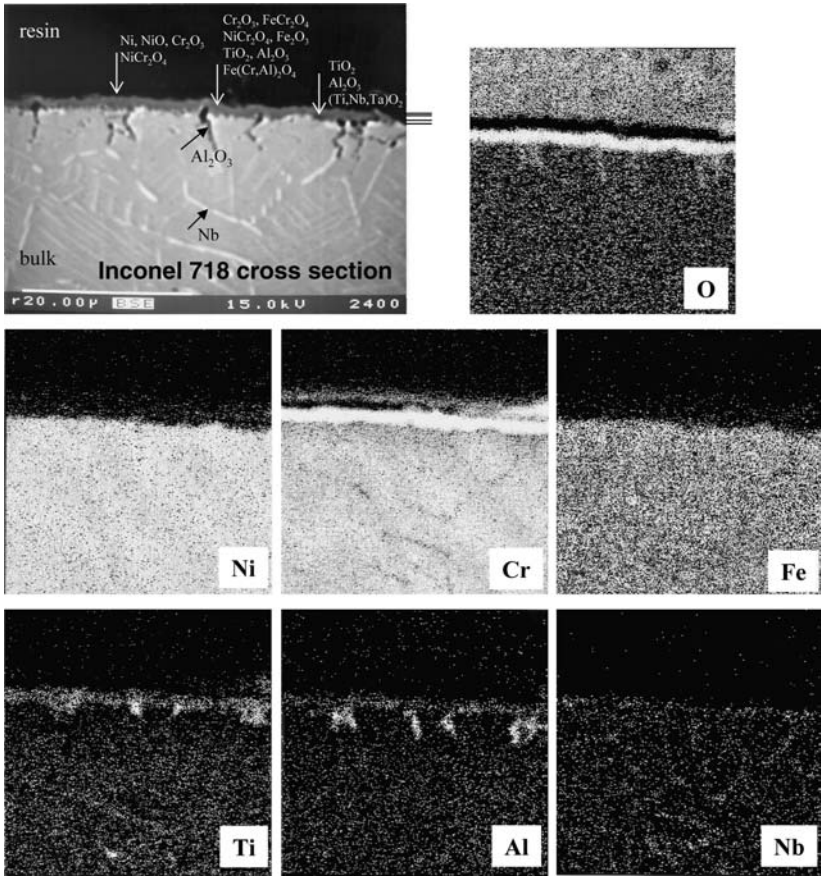

Fig. 6. EPMA back-scattered image for cross section of Inconel 718 showing oxide layers and elemental map images after 24 hr oxidation of alloy specimen at 900°C under 150 mL/min O_2 flow.

Figure 10a shows the TPO profiles for the carbon deposits formed at 600°C on as-received surfaces of Inconel 600, Inconel 718, and Inconel X750 alloys. The CO_2 evolution from Inconel 600 surface is much higher in quantity than that of Inconel 718 and Inconel X750. Four peaks were observed in the TPO profiles of the deposited Inconel 600 surface. The small peak at 150°C results from the oxidation of trapped hydrocarbons in the porous structure of the deposit. The second and third peaks that appear at approximately 375 and 500°C are attributed to the oxidation of amorphous solid deposits, as will be discussed later. The fourth

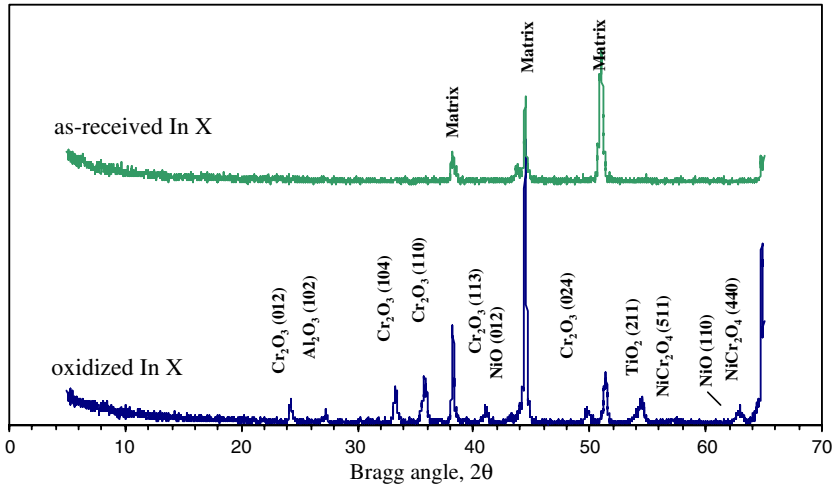

Fig. 7. X-ray diffraction patterns of as-received and oxidized Inconel X foils. Cu Kα ($\lambda = 1.5418$ Å) 40 kV–20 mA.

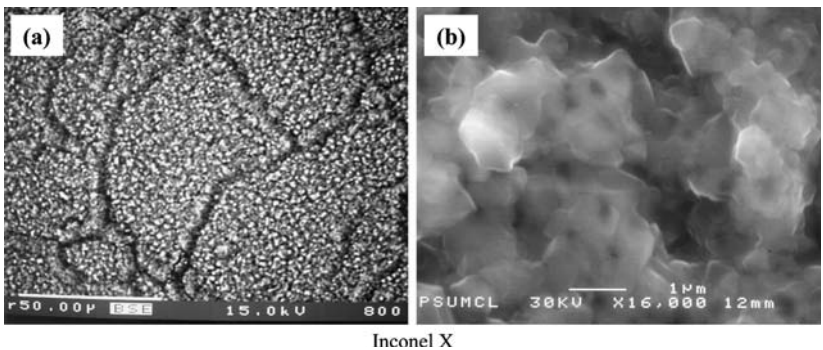

Fig. 8. EPMA back-scattered (×800) (a) and FESEM (×16, 000) (b) images of Inconel X surface after 24 hr oxidation at 900°C under 150 mL/min of O_2 flow.

peak which evolved at approximately 800°C results from the oxidation of the less reactive (more structurally ordered) filamentous carbon deposits. Compared to Inconel 600, Inconel 718 and Inconel X750 alloys collected less deposit giving a broad TPO peak with maximas at around 425, and 450°C respectively, with a shift to lower temperature compared to that of the larger peak observed in the profile for Inconel 600.

Figure 10b shows the TPO profiles of the deposits obtained on the oxidized alloys. As noted, oxidized alloy surfaces collected much less

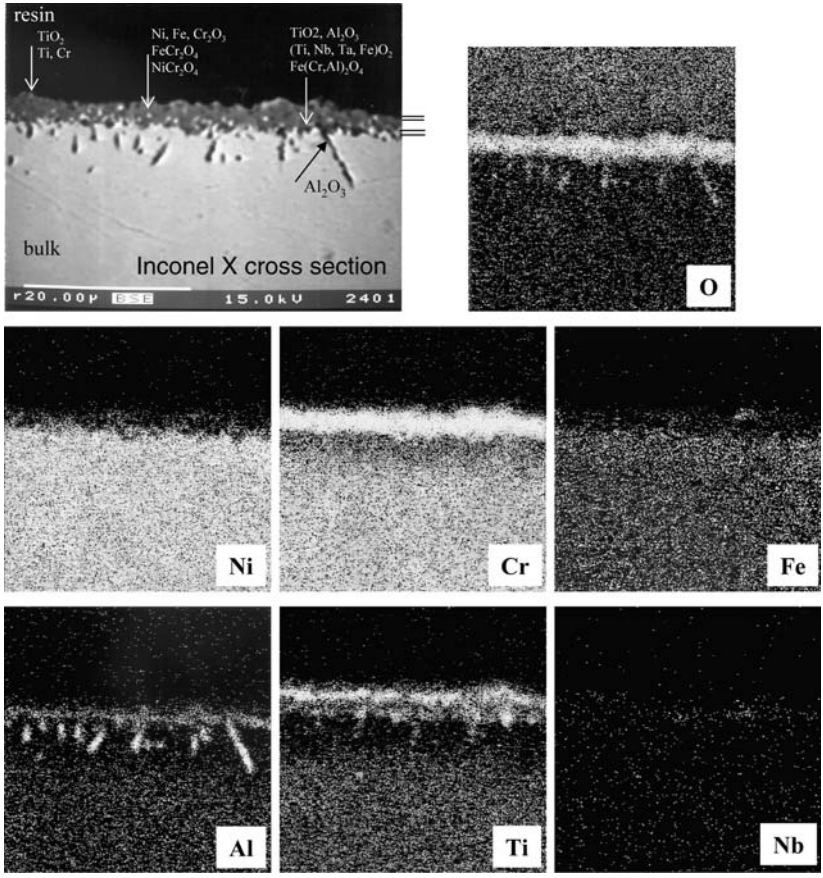

Fig. 9. EPMA back-scattered image for cross section of Inconel X showing oxide layers and elemental map images after 24 hr oxidation of alloy specimen at 900°C under 150 mL/min O_2 flow.

Table II. Total Carbon Deposits Collected on As-received and Oxidized Alloy Surfaces After JP-8 Decomposition at 600°C and 500 psig with 4 cc/min Flow Rate for 5 hr

Alloy	As-received surface (μg/cm^2)	Oxidized surface (μg/cm^2)
In 600	120	35.6
In 718	45	31.2
In X	24	3.2

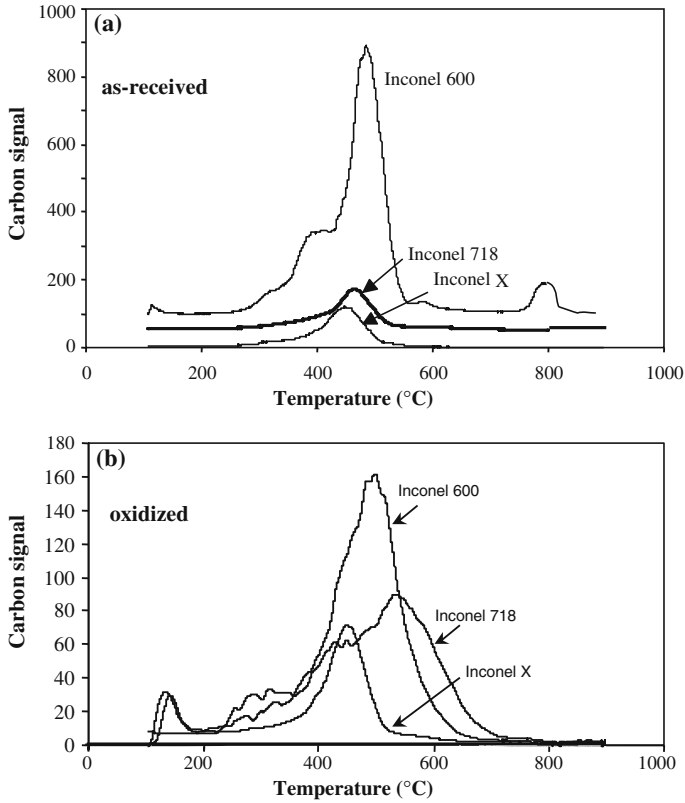

Fig. 10. TPO profiles of carbon deposits from JP-8 decomposition at 600°C and 34 atm (500 psig) for 5 hr at a 4 mL/min flow rate on as-received (a) and oxidized (at 900°C under 150 mL/min O_2 flow for 24 hr) (b) samples of Inconel 600, Inconel 718, and Inconel X.

carbon deposit than that obtained on the respective as-received surfaces. Further, the TPO profiles of the deposits formed on as-received and pre-oxidized surfaces also looked different. The high-temperature (800°C) peak seen with the deposit on as-received Inconel 600 almost disappeared, while the intensity of the broad peak around 500°C was substantially reduced in the pre-oxidized Inconel 600. The TPO profile of the pre-oxidized Inconel 718 showed a broad peak that shifted to higher temperatures compared to that observed with the as-received foil. This observation suggests that the oxidation treatment led to the formation of a less reactive (or more structurally ordered) deposits on the pre-oxidized Inconel 718, although the overall amount of the carbon deposit was reduced. The

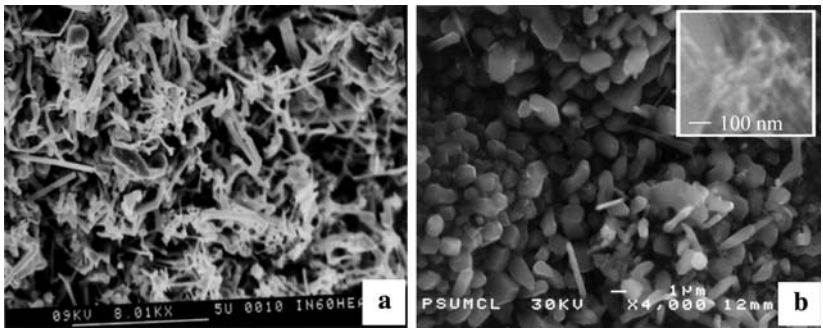

Fig. 11. SEM micrographs of carbon deposits from JP-8 stressing at 600°C and 34 atm for 5 hr on as-received (a) and oxidized (b) Inconel 600 surfaces. The inset in (b) is showing filament formation on oxidized Inconel 600 surface.

profile of Inconel X750 shows one peak centered around 450°C, as seen with the as-received surface. The oxidation treatment reduced the overall carbon deposition on Inconel X750 also, and the effect was intermediate between those seen with the Inconel 600 and 718 samples.

The FESEM examination of the as-received Inconel 600 foil stressed with the jet fuel showed extensive formation of metal sulfide, as seen in Fig. 11a., after 5 hr thermal stressing of JP-8 fuel at 600°C. The XRD analysis indicated that $Ni_{1-x}S$ and $Fe_{1-x}S$ constitute the majority of the metal sulfides formed on the In 600 surface. As expected, the formation of needle-like crystallites roughened the surface and increased the surface area that is accessible to carbon deposition. In contrast, the pre-oxidized Inconel 600 surface, produced insignificant quantities of metal sulfides that are larger in size, as shown in Fig. 11b. No filamentous carbon particles were observed on this surface. The TPO of the deposits collected on the oxidized In 600 (Fig. 10b) did not show a high-temperature peak, confirming the absence of filamentous carbon. In contrast, the TPO profile of the deposit obtained on the as-received surface (Fig. 10a) showed a high-temperature peak around 800°C. These observations indicate that the oxidation treatment has substantially reduced the catalytic activity of the Inconel 600 surface that leads to filamentous carbon formation.

Figure 12 shows the FESEM images of the deposits formed on as-received and oxidized surfaces of Inconel 718. The deposits formed on as-received surface are in the form of metal sulfide crystallites that are 1 and 2 μ in size (Fig. 12a). As-received Inconel 718 surface suffered from $Ni_{1-x}S$ and $Fe_{1-x}S$ formation after thermal stressing with the jet fuel. Traces of small filaments were also observed, in addition to the crystalline deposits. The oxidized surface, however, showed isolated colonies of

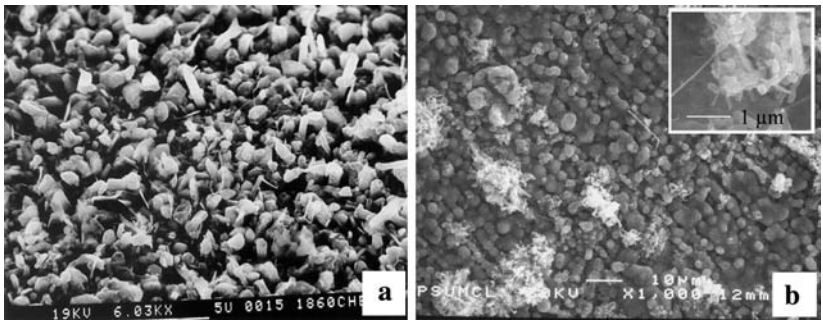

Fig. 12. SEM micrographs of carbon deposits from JP-8 stressing at 600°C and 34 atm for 5 hr on as-received (a) and oxidized (b) Inconel 718 surfaces. The inset in (b) is showing filament formation on oxidized Inconel 718 surface.

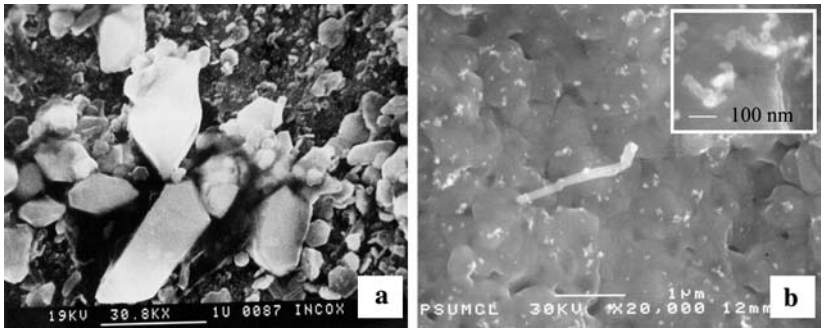

Fig. 13. SEM micrographs of carbon deposits from JP-8 stressing at 600°C and 34 atm for 5 hr on as-received (a) and oxidized (b) Inconel X surfaces. The inset in (b) is showing filament formation on oxidized Inconel X surface.

filamentous carbon, as shown in Fig. 12b. The small inset image in Fig. 12b shows the different sizes of filaments formed at 600°C. The diameter of the filaments ranges between 0.1 and 0.4 μ. In contrast to the observations with Inconel 600, it appears that the oxidation treatment created active sites on the surface of Inconel 718 that catalyze the filamentous carbon formation. These observations are consistent with the peak shift to higher temperatures in the TPO profiles indicating the presence of the deposits with relatively more ordered structures on the oxidized alloy (Fig. 10a and b). Elemental Ni identified at the top of the oxide layer (Fig. 6) may be responsible for this activity. In a similar study, Millward *et al.*[34] reported the formation of filamentous carbon deposits from CO_2 (1%CO) and 1000 ppm C_2H_4 mixture at 550°C on pre-oxidized 20Cr–25Ni–Nb austenitic steels at 550°C in $Ar/H_2/H_2O$.

Similar to Inconel 718, the Inconel X750 surface reacted with the sulfur compounds in jet fuel to produce metal sulfides (Fig. 13a), but not as much as that seen on the Inconel 600 surface. The oxidation of Inconel X750 surface significantly improved its resistance against metal sulfide formation as seen in the micrograph of Fig. 13b. Neither FESEM examination, nor XRD analysis showed any evidence of metal sulfide formation upon stressing the oxidized Inconel X750 with the jet fuel. The oxidation treatment, did, however, change the carbon deposit morphology. As seen with Inconel 718, the deposit on the oxidized Inconel X750 surface contained small filaments.

DISCUSSION

Oxidation of Alloys

The oxidation of the three Inconel alloys produced different oxide phases and structures depending, to some extent, on their elemental composition. The oxidation of Inconel 600 resulted in the formation of relatively stable NiO and Cr_2O_3 phases combined with the $NiCr_2O_4$ spinel, as shown in Figs. 1–3. Since the outer layer contains more NiO, Fe_2O_3, and Ni–Cr spinel, this layer can be easily reduced in the presence of reactive organo-sulfur compounds and hydrocarbons especially at higher temperatures. But just below this outermost layer, a fairly thick and highly stable Cr_2O_3 is present. Compared to Inconel 718 and Inconel X750, Inconel 600 alloy contains a higher concentration of Mn (1%). A significantly high concentration of Mn was observed in the EPMA mapping images of the oxidized Inconel 600 surface (Fig. 3). The relatively high content of Cr and Mn in the top layers may result in the formation of $MnCr_2O_4$[35] at the oxygen-alloy interface. Increase in the Mn content may cause a greater extent of spalling and nodular growth formation.[36] The Fe_2O_3 and $FeCr_2O_4$ spinel formation on the oxidized Inconel 600 surface was not as extensive as that observed on the oxidized Inconel X750 surface.

As seen in the XRD patterns (Figs. 1 and 7) and EPMA images (Figs. 2 and 8), the oxidized Inconel X750 surface has more distinctive grain boundaries and smaller Cr_2O_3 nodules than those seen on the Inconel 600 surface. The outermost layer of Inconel X750 consists of TiO_2 with a lower concentration of Cr_2O_3. Underneath this layer, there is a thick Cr_2O_3 layer with traces of Ni, Fe, and Ti oxides, and $FeCr_2O_4$ and $NiCr_2O_4$ spinels. In this intermediate layer, Ti is probably distributed in the entire region as a dissolved species. The innermost layer is highly enriched in TiO_2, Al_2O_3, and solid solution oxides of (Ti, Nb, Ta)O_2. Litz *et al.*[37] studied the oxidation of Inconel 738 LC and reported significant

Ti diffusion through the entire scale to form a top layer. According to the authors, the formation of outer TiO_2 takes place because Cr_2O_3 dissolves a significant amount of Ti. Therefore, the thickness of the outer TiO_2 layer is controlled by Ti diffusion through Cr_2O_3. The diffusion and oxidation of Nb and Ta are difficult at 900°C. Kumar *et al.*[19] studied the oxidation of Inconel 625 and reported that at temperatures below 1000°C, the solubility of Nb is very low, and the Nb enrichment on the surface increases with the increasing temperature.

As seen in Fig. 6, the oxidation of Inconel 718 resulted in the formation of three noticeable layers. The top layer contains mostly NiO, Cr_2O_3, and $NiCr_2O_4$ but they did not form a dense film similar to that seen with Inconel 600 alloy. Mo did not show any important effect on oxidation behavior of Inconel 718, although it is one of the most important minor components. The intermediate layer is a continuous film of Cr_2O_3, Al_2O_3, Fe_2O_3, $FeCr_2O_4$, $NiCr_2O_4$, and TiO_2. The thickness of the Cr_2O_3 layer is about almost half of those seen in oxidized Inconel 600 and Inconel X750 alloys, although the bulk Cr content of Inconel 718 is 3.5% higher than that of the other two Inconel alloys. The limited growth of the Cr_2O_3 layer can be attributed to the reduced oxygen diffusion by the formation of an Al_2O_3 phase. Since the diffusion of Al to the surface is slow, Al_2O_3 precipitates out as an internal oxide, and, thus, influences the rate of oxidation. The Al content of Inconel 718 is almost the same as that of Inconel X750, but Inconel X750 has a higher Ti content. Since Ti can diffuse faster to the surface through dissolution in Cr_2O_3, a stable TiO_2 layer was obtained on the outermost surface of the oxidized Inconel X750. Similar to the behavior of oxidized Inconel 718, Ti forms two oxide layers, internal and external, on Inconel X750 surface. Therefore, it appears that the ratio of Ti/Al is an important parameter that controls the formation of a stable top layer (TiO_2) upon oxidation of superalloys. Abe *et al.*[38] studied the oxidation of a Ni-based superalloy (19% Cr, 2.13% Al ad 2.49% Ti) containing the same amount of Ti and Al (2.4%) and reported that Ti forms oxides both internally and externally, whereas Al forms only internal oxides in the alloy matrix.

Another important parameter that limits the oxidation rate of Inconel 718 is the higher concentration of Nb and Ta. Elliot and Hampton[24] have shown that the addition of 7.7% Nb to Ni–10%Cr significantly improves the oxidation resistance of the alloy. The authors reported that the oxidation rate decreased almost 50% after adding Nb to the Ni–Cr alloy. As can be seen in Fig. 6, the Nb concentration increased in the innermost layer. Kumar *et al.*[19] reported that the diffusion coefficient of Nb is larger than that of Cr over the entire range of oxidation temperatures (1050–1250°C) during the oxidation of Inconel 625 alloy. The enrichment

of Nb, Ta, and Al oxides near the surface can control the oxygen diffusion through the bulk and, thus, limit the thickness of the stable oxide layer.

Jet Fuel Stressing on As-received and Oxidized Alloys

Few studies[39–41] were reported on the carbon deposition from hydrocarbons on the surface of oxidized Ni–Cr–Fe alloys. Some of Ni and Fe oxides can be readily reduced to become active catalysts for carbon deposition.[42] The results of TPO profiles and FESEM images of both as-received and oxidized alloys have indicated that the metal sulfide formation and carbon deposition on oxidized surfaces were reduced significantly compared to that obtained on as-received surfaces. The reduced deposition can be attributed to the formation of thermodynamically stable oxides on alloy surfaces. It is well known that Ni, Fe, and Co have a strong tendency to form their sulfides by reacting with the sulfur compounds in the fuel, and they also catalyze carbon deposit formation by producing filamentous carbon. This type of deposit is the most detrimental, causing extensive surface damage. The formation of thermally stable oxide coatings, like Al_2O_3, TiO_2, and Cr_2O_3 can reduce the catalytic effect of these metals under hydrocarbon stressing conditions up to 600°C. Based on the Gibbs free energy for the oxidation reaction, the termodynamic stabilities of some metal oxides fall in the following descending order:[19,43]

$$Ta_2O_5 > Nb_2O_5 > Al_2O_3 > Cr_2O_3 > Fe_3O_4 > TiO_2 > SiO_2 > NbO_2 > Fe_2O_3 > MoO_2 > FeO > NiO$$

Thermal stressing of jet fuel at 600°C leads to the pyrolysis of less stable hydrocarbons and produce highly reactive hydrocarbon radicals, such as $CH_2\bullet$, $CH_3\bullet$. These hydrocarbon radicals can reduce the surface oxides by abstracting oxygen, producing active metal sites that catalyze dehydrogenation of adsorbed hydrocarbon species to produce elemental carbon. Carbon atoms will, then, react with the reduced metal surface to form metal carbide crystals and/or lead to filamentous carbon formation. The electronic and structural properties of metal surfaces control the dissociation of hydrocarbons and diffusion of elemental carbon.[6]

The TPO profiles (Fig. 10a) and electron microscope images (Figs. 11a, 12a, and 13a) of the as-received surfaces indicate that the surface consists mostly of Ni and Fe sulfides and carbon deposits on the Inconel 600 alloy surface; filamentous carbon deposits and columnar and platelet-type metal sulfide/carbide crystals on the Inconel 718; metal sulfide/carbide crystallites on the Inconel X750 surfacess. Similar catalytic platelet structures produced by catalytically active surfaces were observed by Sacco

and co-workers[44,45] on Fe, Ni, and Co foil surfaces after increasing the O/H ratio in the $CO–CO_2–CH_4–H_2$ gas mixture at 625°C. They concluded that CO might be responsible for the formation of platelet carbon deposits which have been postulated to form upon cooling of the metal matrix that is either saturated with carbon or has formed a carbidic layer. The catalytic activity of Inconel 600 alloy is much higher than that of the other two alloys. In addition to the microstructural effect (γ and γ' phases), elemental composition of these alloys play the most important role in controlling the degree of carbon deposition. In our previous study,[46] the initial stages of oxidation (<30 min, T = 800°C) of Inconel 600 and Inconel 718 surfaces enriched Cr and depleted Ni on the surface, as indicated by the XPS analysis. These compositional changes improved the resistance of the alloy surfaces to carbon deposit formation from jet fuel decomposition. In this study, the 24 hr oxidation of Inconel 600, Inconel 718, and Inconel X750 surfaces produced thermally stable layers of Cr, Ti, and Al oxides and (Ni, Fe)Cr_2O_4 spinels. The solubility and diffusion of carbon through the alloys play an important role in the formation of carbonaceous deposits and metal carbides. It has been demonstrated that oxide formation on the surface of the alloy decreases the solubility of carbon.[47]

The comparison of TPO profiles with respect to peak intensity and peak positions provides some information on the nature of the carbon deposits and the activity of the substrate surfaces.[8] For example, the peaks that evolved at 400 and 775°C in the as-received Inconel 600 did not appear in the TPO of the deposits obtained on the oxidized surface, and the absence of the high temperature peak at 775°C indicates the lowered catalytic activity upon oxidation (Figs. 10a and b). Thermal stressing after oxidation of Inconel 600 surface lowered the intensity of the maximum peak at 500°C (Figs. 10a and b), also indicating a reduced surface activity for deposition. The TPO profiles of the as-received and oxidized Inconel 718 showed an approximately 75°C shift in the peak temperature in the TPO profile of the oxidized sample to higher temperatures. This shift indicates that the deposit collected on the oxidized Inconel 718 surface is relatively more difficult to oxidize. This may result from deposition in the pores and cracks produced after the oxidation, and the presence of elemental nickel seen on the surface. The TPO profiles of the as-received and oxidized Inconel X750 surfaces do not show much difference in the peak positions. The CO_2 signal intensity of the oxidized specimen is almost half of the as-received sample. The TPO profile in Fig. 10b gave a single peak suggesting a uniform activity on the surface, and the absence of cracks or pores on the oxidized Inconel X750 surfaces.

The FESEM images in Figs. 11b, 12b, and 13b of the carbon deposit morphologies on the oxidized alloy surfaces can explain the behavior

of the oxidized surface upon thermal stressing. On the oxidized Inconel 600 surface, the metal sulfide formations are in the form of large crystals that are dislocated from the surface through the gas phase side. Figueiredo[48] observed similar crystal deposit structures after steaming the carbon deposited surface of the alloy 36XS (Fe–Ni–Cr alloy). There are also some traces of small carbon filaments in isolated areas of the surface. Compared to the oxidized Inconel 600 surface, the oxidized Inconel 718 and Inconel X750 surfaces did not produce significant Ni and Fe sulfides or collect heavy carbon deposits. Although the surface topography of the oxidized Inconel 600 changed significantly after the fuel stressing, no change was observed on the oxidized Inconel 718 and Inconel X750. On the oxidized Inconel 718 surface, more filamentous deposit growth was observed when compared to the oxidized Inconel X750. The filamentous carbon deposits on all these three alloy surfaces at 600°C grew without the presence of metallic particles at the tip of the filaments implying that the metal catalyst particles remain embedded in the alloy surface. The deposits formed on Inconel 718 seem to grow on some catalytically active sites produced by the reduction of NiO and Fe_2O_3. The spinel formation ($FeCr_2O_4$, $NiCr_2O_4$, and $MnCr_2O_4$) on both oxidized Inconel 600 and Inconel 718 surfaces may also affect the filament formation. For instance, the presence of chromium in mixed spinel oxides reduced the formation of dense carbon and inhibits filamentous carbon, but iron act as a catalyst for filamentous grwoth in Mn–Fe–Cr spinels.[49] Steurbaut *et al.*[50] studied thermal cracking of $C_2H_6/C_2H_4/H_2$ mixture at a temperature of 850°C on pre-oxidized HP40 alloy and reported that coke formation was initiated by the reduction of (Fe, Ni, Cr)-spinels which gives rise to the formation of (Fe,Ni)-particles showing strong catalytic activity. The filamentous deposits formed on Inconel 718 surface, in Fig. 12b, are in various diameters indicating a range of catalytically active particle sizes. Different deposit size formation can be also easily detected from the number of peaks and broadening of TPO profile in Fig. 10b. On the other hand, as seen in Fig. 13b Inconel X750 surface produced almost uniform deposits of 100 nm in length and 50 nm in diameter. Therefore, it can be presumed that the formation of TiO_2 on Inconel X750 changed the deposit morphology significantly, and the presence of NiO is probably responsible from the formation of the catalytically formed small filaments. The TiO_2 itself did not produce any filamentous type deposit from JP-8 decomposition at 600°C, only spherical amorphous type deposits were observed in our previous study[51]. Baker[52] reported that adding TiO_2 to Ni–Fe containing catalyst sample for acetylene decomposition at 850°C reduced the filamentous deposit formation to the half of the quantity produced by the Ni–Fe sample. Thus, the formation of TiO_2 rich layer on oxidized Inconel

X750 is most probably responsible for the decreased deposit formation. Presumably, active metals like, Ni and Fe in the form of oxides and spinels are dispersed throughout the TiO_2 layer causing filamentous carbon formation.

The lower extents of carbon deposition on the as-received and oxidized Inconel X750 compared to those of Inconel 718 may be attributed to the differences in their elemental composition and microstructure. In addition to differences in the Ni contents of Inconel 718 and Inconel X750 alloys, Ti/Al ratio could be considered as another important parameter that affects the deposit formation particularly after the oxidation of the alloy surfaces. The Ti/Al ratios are 1.8 and 3.6 for Inconel 718 and Inconel X750, respectively. Higher Ti content seems to facilitate the formation of a denser and crack free TiO_2 layer, as evidenced in Fig. 8 by a fine-grained and well-adherent oxide scale formed on the Inconel X750 surface after oxidation. In contrast, as shown in Fig. 5, the oxidation of the Inconel 718 surface produced an oxide scale which tends to spall off from the surface. Grabke *et al.*,[53] studied the carbon uptake on oxidized Fe–6Al and Fe–6Al–0.5Ti alloys and reported that the former alloy did not produce a well adherent Al_2O_3 scale, but the later produced an adherent, crack free, and ductile TiO_2 layer. Furthermore, the presence of Ti in the Al_2O_3 may improve the ductility of the oxide. The authors also reported that cracks could be formed by oxide growth stresses, during creep or upon thermal and/or mechanical cycling. In this case, carbon might also permeate through the imperfections of the scale, pores, dislocation cracks, perhaps grain boundaries. Thus, it appears that Inconel X750 with a higher Ti content produced a crack and defect free surface impermeable to deposit precursors from the jet fuel decomposition. Furthermore, the lower Cr content of Inconel X750 (Cr 15.5%) compared to In 718 (Cr 19.0%) increased the concentration of TiO_2 and Al_2O_3 in the top scale contributing to the formation of an effective oxide layer against sulfide formation. It has been shown that in sulfur containing atmospheres at high temperature, the Al_2O_3—forming alloys perform better than the Cr_2O_3—forming alloys.[54]

The average grain boundary size of Inconel X750 (50 μ) is larger than that of Inconel 718 (10 μ). Larger grain size would impede the diffusion of Cr to the surface to form a Cr_2O_3 layer on the surface. In contrast, alloys with small grain sizes have more boundaries for Cr to diffuse to the surface. Also, the presence of small grain sizes would allow the penetration of C through cracks and pores produced during the formation of Cr oxide rich grains.

As Forseth and Kofstad[55] and Grapke *et al.*[56] reported that the initial carbide formation probably starts with the formation of chromium

carbide, then the alloy matrix becomes depleted in Cr as carbon is continuously supplied at the surface and diffuses into alloy. Especially on both as-received and oxidized Inconel 600 surfaces (Figs. 11a and b), the carbide growth continuous gradually by incorporating Fe, the matrix become a binary Fe–Ni alloy. The Fe-carbide formation increased the Ni content on the surface. Finally, Fe–Ni carbides decompose to metal particles and carbon to catalyze filamentous deposit formation as seen in the inset of Fig. 11b.

After jet fuel thermal stressing, the deposited alloy samples were again examined by EPMA for any deep carbon attack and change in the cross section. There was no serious deep attack observed on any of the foils from the carbon map. Only on the outer surface of Inconel 600, approximately 1–2 μ thick carbon corrosion traces were observed from the EPMA cross-section view. This penetration probably resulted from the formation of columnar crystalline structures that are approximately 2 μ thick. In addition, the XRD pattern of the deposited Inconel 600 surface gave traces of metal carbides such as Ni_3C, Fe_7C_3, Fe_5C_2 and Fe_3C and sulfide in FeS form. Similar iron carbide, Fe_7C_3 and Fe_5C_2, crystal formations were also reported to form during CO disproportionation on Fe at 500°C.[55]

CONCLUSIONS

The results from this study have shown that the oxidation treatment reduced the overall metal sulfide formation and carbon deposition on the superalloy surfaces and changed the nature of the deposits formed on these surfaces, as well. Changes on superalloy surface composition upon oxidation, and their subsequent effects on the amount and nature of carbon deposit appear to depend strongly on the composition and metallurgical characteristics of the starting alloys. In particular, the minor elements present in small concentrations play an important role during oxidation and the behavior of the oxidized surface during thermal stressing with jet fuel.

The oxidation of Ni-based superalloys produced oxide films covering the entire surface of the alloy coupons. The type of metal oxide formation and the oxide layer thickness depend on the alloy composition. The Inconel 600 produced mainly three layers of oxides (NiO, Fe_2O_3, Cr_2O_3) including spinels ($MnCr_2O_4$, $NiCr_2O_4$, and $FeCr_2O_4$). The total thickness of the oxide layer approached approximately 8 μm on the Inconel 600 surface. The Inconel 718, on the other hand, produced thinner oxide layers composed of NiO, Fe_2O_3, Cr_2O_3, Al_2O_3, and TiO_2, spinels ($NiCr_2O_4$ and $FeCr_2O_4$), and solid solution of (Ti, Nb, Ta, Fe)O_2. The total thickness of

the oxide layer on the Inconel 718 surface was approximately 4 μm. The Inconel X750 produced a TiO_2 layer on top of the NiO, Fe_2O_3, Cr_2O_3, spinels and solid solution of (Ti, Nb, Ta)O_2. The total thickness of the oxide layers on Inconel X750 was approximately 10 μm, the thickest layer of oxides among three alloys.

The pre-oxidation of Inconel alloys at 900°C significantly reduced the metal sulfide and carbon deposit formation upon thermal stressing with JP-8 at 600°C and 34 atm for 5 hr. Thermal stressing produced 120 $\mu g/cm^2$ deposit on as-received Inconel 600 surface, compared to 35.6 $\mu g/cm^2$ obtained on the pre-oxidized surface. Although to a lesser extent, reduction in carbon deposition was also observed on the other two Inconel alloys after the pre-oxidation. The pre-oxidized Inconel X750 surface inhibited the metal sulfide formation significantly due to the formation of TiO_2 layer in the gas–solid interface. A significant reduction in the sulfidation rates of the Inconel alloys was achieved by pre-oxidizing. On all pre-oxidized surfaces, filamentous carbon formation (catalyzed by metals) was reduced after producing thermally stable oxide layers with reduced diffusion of carbon precursors through the metal matrix.

EPMA results showed that, after 5 hr thermal stressing with JP-8 on alloy surfaces carbon precursor and metal surface interaction takes place within the top 1 μm oxide layer, and no carbon was observed reaching the intermediate Cr_2O_3 layer.

REFERENCES

1. S. Zabarnick, *Industrial & Engineering Chemistry Research* **33**, 1348 (1994).
2. R. W. Stickles, W. J. Dodds, T. R. Koblish, J. Sager and S. Clouser, *Agard Conf. Proceed. 536*, Fuels and Combustion Technology for Advanced Aircraft Engines, Italy, p. 20–1, May 1993.
3. D. L. Linne, M. L. Meyer, T. Edwards, and D. A. Eitman. AIAA-97–3041.
4. O. Altin and S. Eser, *Industrial & Engineering Chemistry Research* **40**, 642 (2001).
5. R. T. K. Baker and P. S. Harris, in *Chemistry and Physics of Carbon*, P. L. Walker ed. **14**, 83 (1978).
6. M. Ryniers and F. G. Froment, *Industrial & Engineering Chemistry Research* **34**, 773 (1995).
7. L. F. Albright and T. C. H. Tsai, in *Pyrolysis: Theory and Industrial Practice*, L. F. Albright, B. L. Crynes, and W. H. Corcoran eds., Chap. **10**, 233 (1983).
8. M. J. Graff and L. F. Albright, *Carbon* **20**, 319 (1982).
9. O. Altin and S. Eser, *Industrial Engineering Chemistry Research* **40**, 596 (2001).
10. M. Fujita, S. Jomyungyong, Y. Itoh, S. Yokoyama, and S. Matsumoto, *Transactions of the Institute of Metal Finishing*, **75**(3), 98 (1997).
11. K. L. Luthra and D. W. McKee, U. S. Patent, 5,077,140 (1991).
12. W. E. Olson and D. K. Gupta, U. S. Patent, 4,933,239 (1990).
13. O. Altin, A. Venkataraman, and S. Eser, ACS, Div. Pet. Chem. 216th Nat. Meet. **43**(3), 404 (1998).
14. S. Ibarra, in *Pyrolysis: Theory and Industrial Practice*, L. F. Albright, B. L. Crynes, and W. H. Corcoran eds., Chap. **16**, 427 (1983).

15. R. A. Holm and H. E. Evans, *Materials and Corrosion* **38**, 166 (1987).
16. H. Kutsumi, S. Muneki, T. Itagaki, F. Abe, *Journal of Japanese Institute of Metals* **66**(10), 997 (2002).
17. N. S. McIntyre, D. G. Zetaruk, and D. Owen, *Applied Surface Science* **2**, 55 (1978).
18. M. Lenglet, R. Guillamet, J. Lopitaux, and B. Hannoyer, *Materials Research Bulletin* **25**, 715 (1990).
19. L. Kumar, R. Venkataramani, M. Sundararaman, P. Mukhopahyay, and S. P. Garg, *Oxidation of Metals* **45**(1/2), 221 (1996).
20. M. Durasso and R. L. Ramanathan, *Congresso Anual da ABM* **36**, 353 (1981).
21. C. S. Giggins and F. S. Petit, *Transactions of Metallrgical Society at AIME* **245**, 2495 (1969).
22. J. H. Chen, P. M. Rogers, and J. A. Litte, *Oxidation of Metals* **47**(5/6), (1997).
23. C. T. Sims, N. S. Stoloff, and W. C. Hagel, Superalloys, (John Wiley & Sons, Inc. New York, 1987).
24. P. Elliot and A. F. Hampton, *Oxidation of Metals* **14**, 449 (1980).
25. W. F. Taylor, *Industrial and Engineering Chemistry: Product Research and Development* **15**, 64 (1976).
26. L. J. Velenyi, Y. Song, J. C. Fagley, *Industrial & Engineering Chemistry Research* **31**, 285 (1981).
27. M. F. S. G. Reyners, G. F. Froment, *Industrial Engineering Chemistry Research* **34**, 773 (1995).
28. C. D. Tan and R. T. K. Baker, *Catalysis Today* **63**, 3 (2000).
29. K. Ohla and H. J. Grabke, *Werkstoffe und Korrosion* **33**, 341 (1982).
30. D. L. Trimm and C. J. J. Turner, *Chemical Technology and Biotechnology* **31**, 285 (1981).
31. S. Mrowec, T. Walec, and T. Werber, *Oxidation of Metals* **21**, 925 (1970).
32. K. N. Statford and R. Manifol, *Corrosion Science* **9**, 489 (1969).
33. O. Altin and S. Eser, *Industrial Engineering Chemistry Research* **39**(3), 642 (2000).
34. G. R. Millward, H. E. Evans, M. Aindow, and C. W. Mowforth, *Oxidation of Metals*. **56**(3/4), 231 (2001).
35. D. L. Douglass and F. Rizzo-Assuncao, *Oxidation of Metals* **29**, 272 (1988).
36. N. Hussain, K. A. Shahid, I. H. Khan, and S. Rahman, *Oxidation of Metals* **41**(1/2), 251 (1994).
37. J. Litz, A. Rahmel, M. Schorr, and J. Weiss, *Oxidation of Metals* **32**, 167 (1989).
38. F. Abe, H. Araki, H. Yoshida, and M. Okada, *Oxidation of Metals* **27**(1/2), 21 (1987).
39. G. W. Horsley and J. A. Cairns, *Applied Surface Science* **18**, 273 (1984).
40. J. E. Castle and M. J. Durbin, *Carbon* **13**, 23 (1975).
41. A. L. Marasco and D. J. Young, *Oxidation of Metals* **36**, 157 (1991).
42. A. Tomita, K. Yoshida, Y. Nishiyama, and Y. Tamai, *Carbon* **30**, 601 (1972).
43. L. B. Pankratz, J. M. Stuve, and N. A. Gokcen, Thermodynamic Data for Mineral Technology (U. S. Bureau of Mines. Bull. **No. 677**, 1984).
44. G. A. Jablonski, F. W. Geurts, A. Sacco, Jr, and R. R. Biederman, *Carbon* **30**(1), 87 (1992).
45. G. A. Jablonski, F. W. A. H. Geurts, and A. Sacco, Jr, *Carbon* **30**(1), 99 (1992).
46. O. Altin and S. Eser, manuscript in preparation.
47. I. Wolf and H. J. Grabke, *Solid State Communications* **54**, 5 (1985).
48. J. L. Figueiredo, *Materials and Corrosion* **49**, 373 (1998).
49. G. C. Allen and J. A. Jutson, *Journal of Material Chemistry* **1**(1), 73 (1991).
50. C. Steurbaut, H. J. Grabke, D. Stobbe, F. R. van Buren, S. J. Korf, and J. Defrancq, *Materials and Corrosion* **49**, 352 (1998).
51. F. Zhang, O. Altin, and S. Eser, Carbon'99 24th Biennial Conference on Carbon, Vol. **2**, 814 (1999).
52. Baker (R. T. K. Baker, Carbon Fibers Filaments and Composites, NATO ASI Series, Series E, V. 1117, 405, (1989) (Eds. J. L. Figueiredo, C. A. Bernardo, R. T. K. Baker and K. J. Huttinger).
53. H. J. Grabke, K. Ohla, J. Peters, and I. Wolf, *Werkstoffe und Korrosion* **34**, 495 (1983).

54. H. L. Du, J. Kipkemoi, D. N. Tsipas, and P. K. Datta, *Surface and Coatings Technology* **86–87**, 1 (1996).
55. S. Forseth and P. Kofstad, *Materials and Corrosion*, **46**, 201 (1995).
56. H. J. Grapke, R. Krajak, and E. M. Muller-Lorenz, *Materials and Corrosion* **44**, 89 (1993).